Supplemental Materials

Molecular Biology of the Cell

Krefman et al.

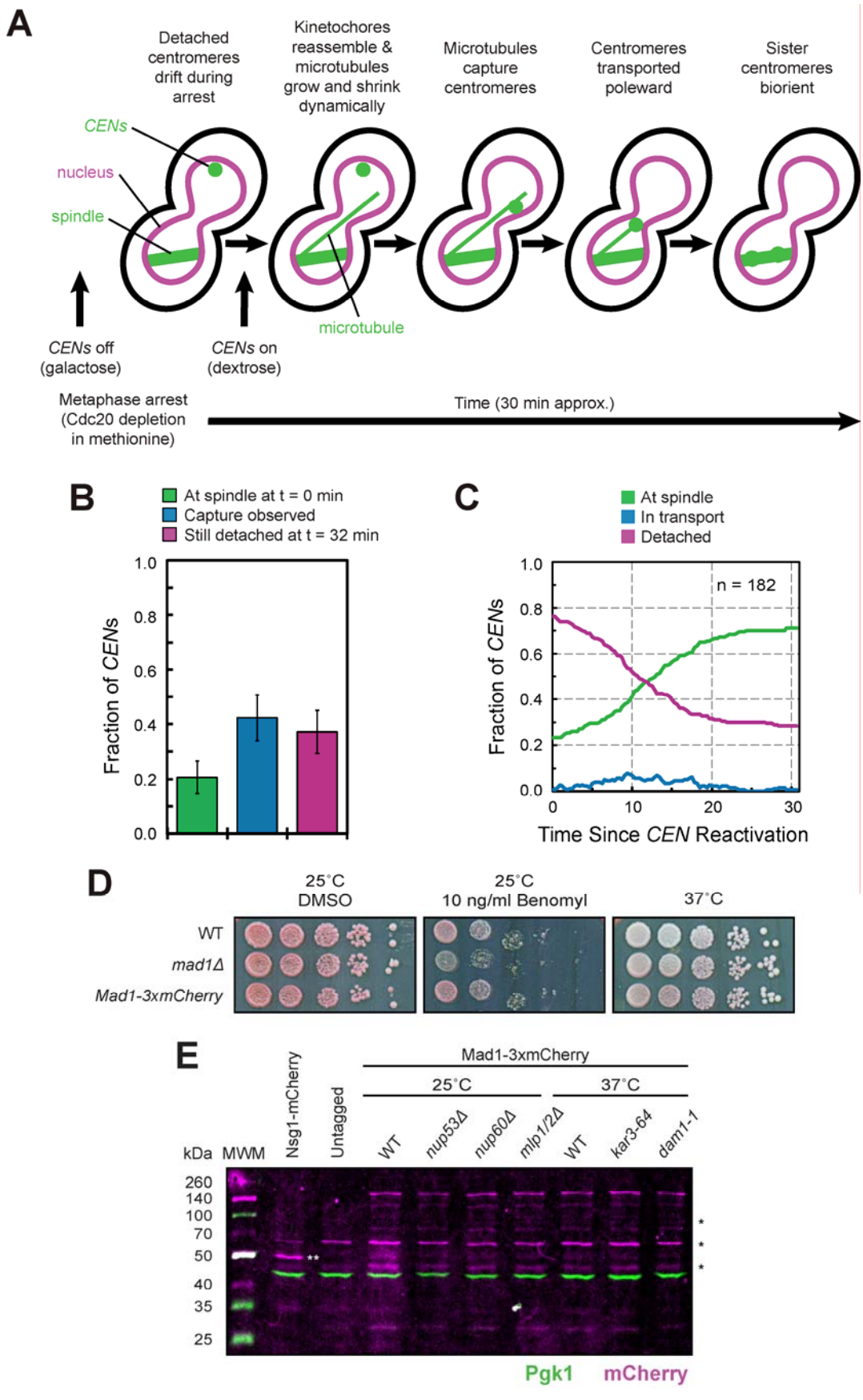
A
Detached centromeres drift during arrest
Kinetochores reassemble & microtubules grow and shrink dynamically
Microtubules capture centromeres
Centromeres transported poleward
Sister centromeres biorient
CENs
nucleus
spindle
microtubule
CENs off (galactose)
CENs on (dextrose)
Metaphase arrest (Cdc20 depletion in methionine)
Time (30 min approx.)
B
At spindle at t = 0 min
Capture observed
Still detached at t = 32 min
Fraction of CENs
C
At spindle
In transport
Detached
n = 182
Fraction of CENs
Time Since CEN Reactivation
D
25°C DMSO
25°C 10 ng/ml Benomyl
37°C
WT
mad1Δ
Mad1-3xmCherry
E
Mad1-3xmCherry
25°C
37°C
Nsg1-mCherry
Untagged
WT
nup53Δ
nup60Δ
mlp1/2Δ
WT
kar3-64
dam1-1
kDa MWM
260
140
100
70
50
40
35
25
Pgk1
mCherry

Figure S1. The centromere reactivation assay for analysis of Mad1 localization to kinetochores.
(A) The centromere reactivation assay. Cells are arrested in metaphase by depletion of the APC component Cdc20 controlled by the methionine-repressible *MET3* promoter (*MET3pr-CDC20*). One pair of sister centromeres is controlled by a *GAL1* promoter integrated adjacent to the centromere of Chromosome 3 and is visualized with TetR-GFP (*GAL1pr-CEN3-TetOs*). In the presence of galactose, transcription across *CEN3* displaces kinetochore proteins, detaching the sister chromatids from the spindle. *CEN3* is then reactivated by the addition of dextrose, repressing transcription across the centromeres and allowing kinetochores to reassemble. Cartoon is based on (Tanaka *et al.*, 2010). **(B-C)** Analysis of capture following centromere reactivation in strains expressing GFP-Tub1 and TetR-GFP. Live cells were continuously observed for 32 min by epifluorescence microscopy. **(B)** Frequency of capture. Mean of three independent experiments is shown. Error bars represent SD. **(C)** Progress of centromere capture and retrieval during one experiment. **(D)** Serial dilutions of wild-type, *mad1Δ*, and *MAD1-3×mCherry* yeast. **(E)** Immunoblot against mCherry and Pgk1 (loading control) in lysates of the centromere reactivation strains used in this study. Asterisks indicate background bands detected in all strains.

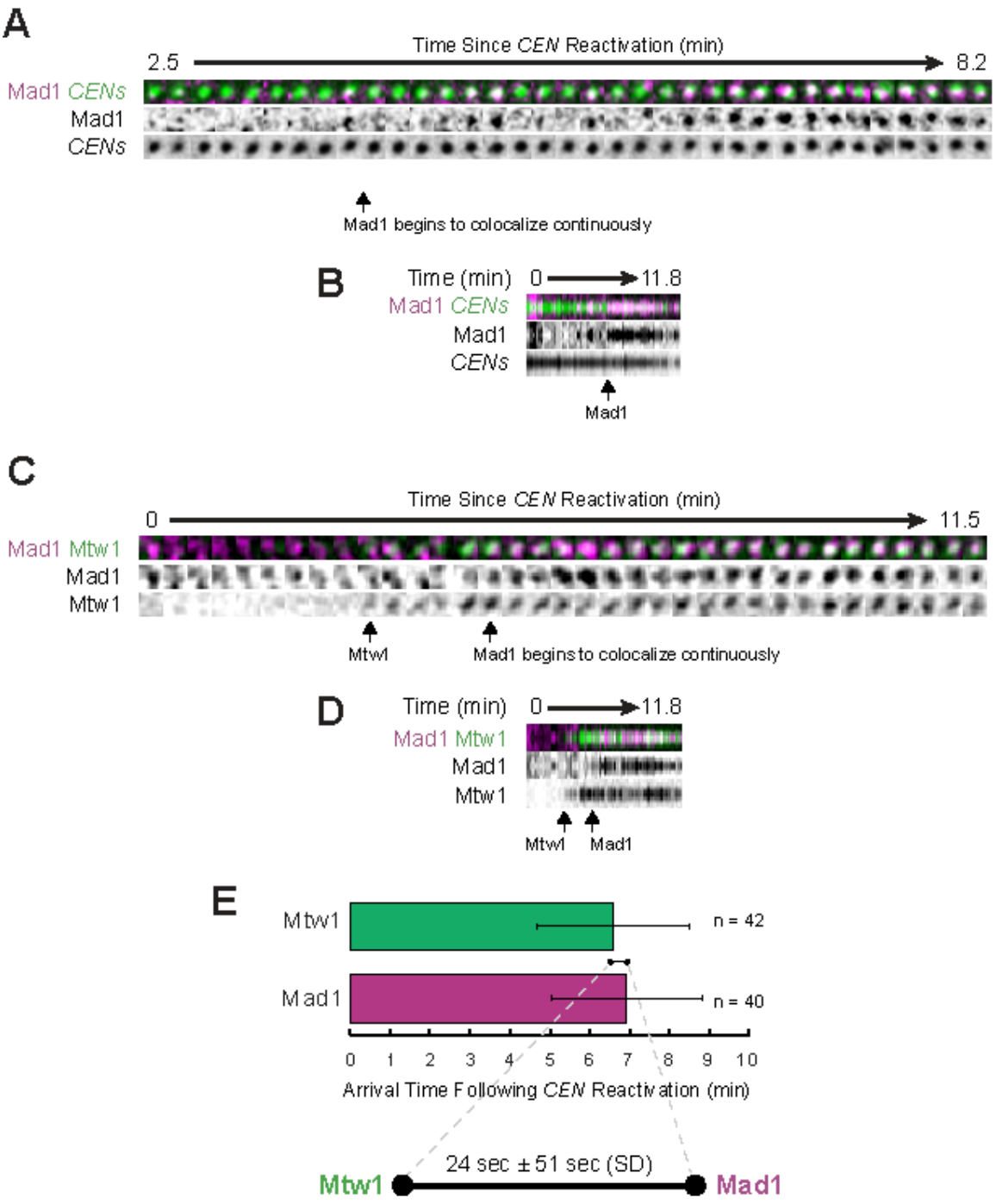

Figure S2. Mad1 and Mtw1 appearance after centromere reactivation.
Additional data from the cells shown in Figure 1A-B and Video 1-2. **(A)** Time series centered on the centromere of the cell in Figure 1A and Video 1 to show the accumulation of Mad1 (10 sec/frame). **(B)** Kymograph of the spot series in (A). **(C)** Time series centered on the centromere of the cell in Figure 1B and Video 2 to show the accumulation of Mad1 and Mtw1 (20 sec/frame). **(D)** Kymograph of the spot series in (C). **(E)** Mean arrival time of Mtw1-3×GFP and Mad1-3×mCherry at centromeres

following reactivation. Black barbell shows the average delay between the first appearance of Mtw1 and Mad1.

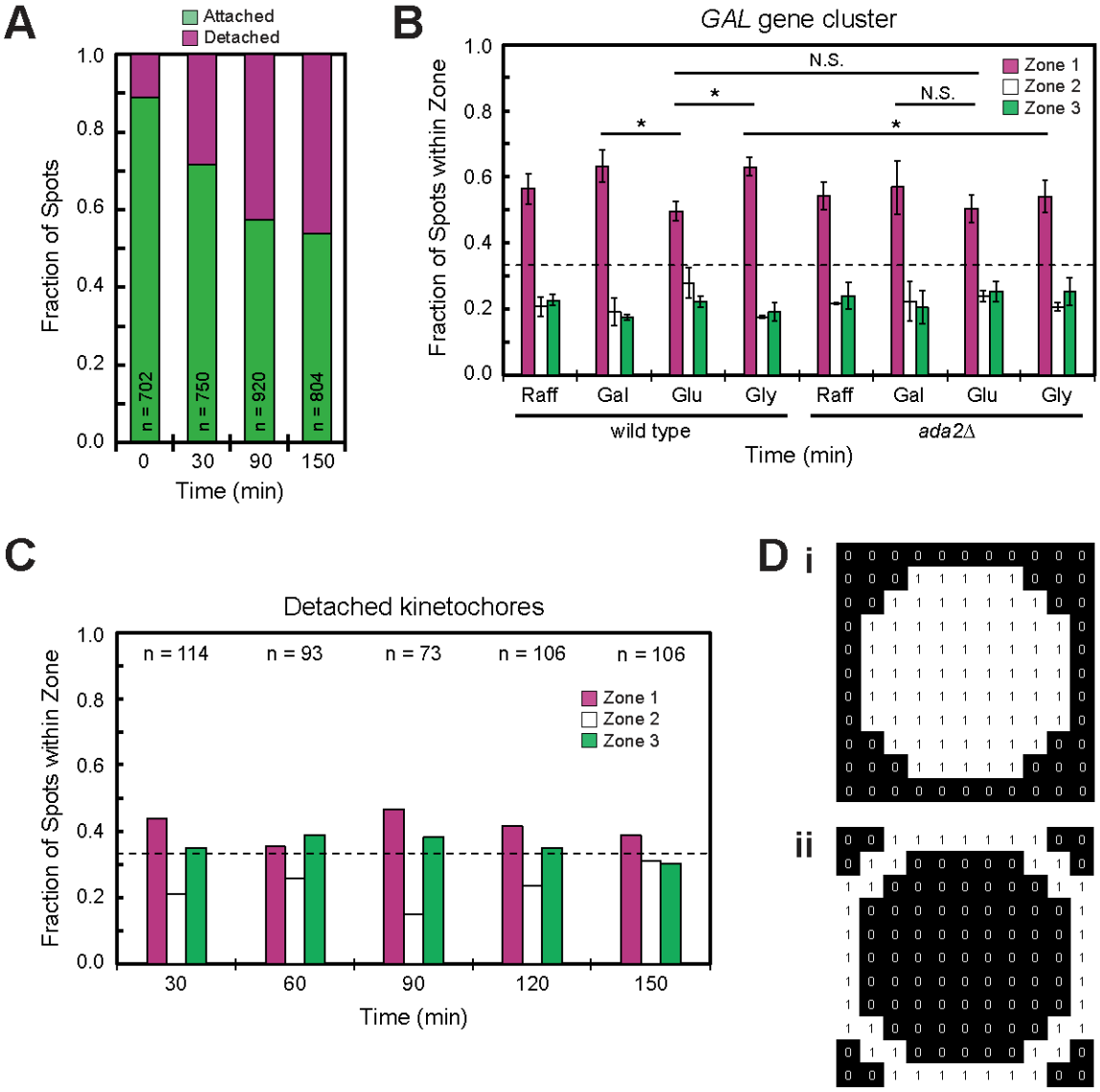

Figure S3. Analyses of the subnuclear localization distribution of detached kinetochores in nocodazole and the *GAL* gene cluster in different carbon source. **(A)** Fraction of Mtw1-3×GFP spots that are associated with Spc42-RFP (attached) or not (detached) in asynchronously dividing cells exposed to nocodazole for 0 to 150 min before fixation and imaging by epifluorescence microscopy. Data are from the same experiment as Figure 4B. **(B)** Subnuclear localization distribution of the *GAL* gene cluster in wild-type and *ada2Δ* cells cultured in the presence of the indicated carbon sources. Our quantification showed that the *GAL* gene cluster is localized peripherally, its peripheral localization was reduced by culturing cells under transcriptionally repressive conditions compared with permissive or inducing conditions, and that cells lacking *ADA2* fail to respond to induction of *GAL* transcription by increasing the localization of the genes to

the periphery. There was no significant difference in *GAL* localization in *ada2Δ* cells grown in galactose versus glucose, and no significant difference in *GAL* localization in glucose between wild-type and *ada2Δ* cells. Our findings agree with those of Cabal et al. (2006) and Green et al. (2012). **(C)** Subnuclear localization distribution of detached kinetochores in cells expressing Mtw1-3×GFP, Spc42-CFP and Nsg1-mCherry, treated as in (A). Spots were localized manually (see Materials and Methods). Dotted lines at 33.3% represent the expected distributions if localization is random. **(D)** Masks for quantification of fluorescence intensity in Figure S4. White pixels (ones) were included, while black pixels (zeros) were excluded. **(i)** Signal mask. **(ii)** Background mask.

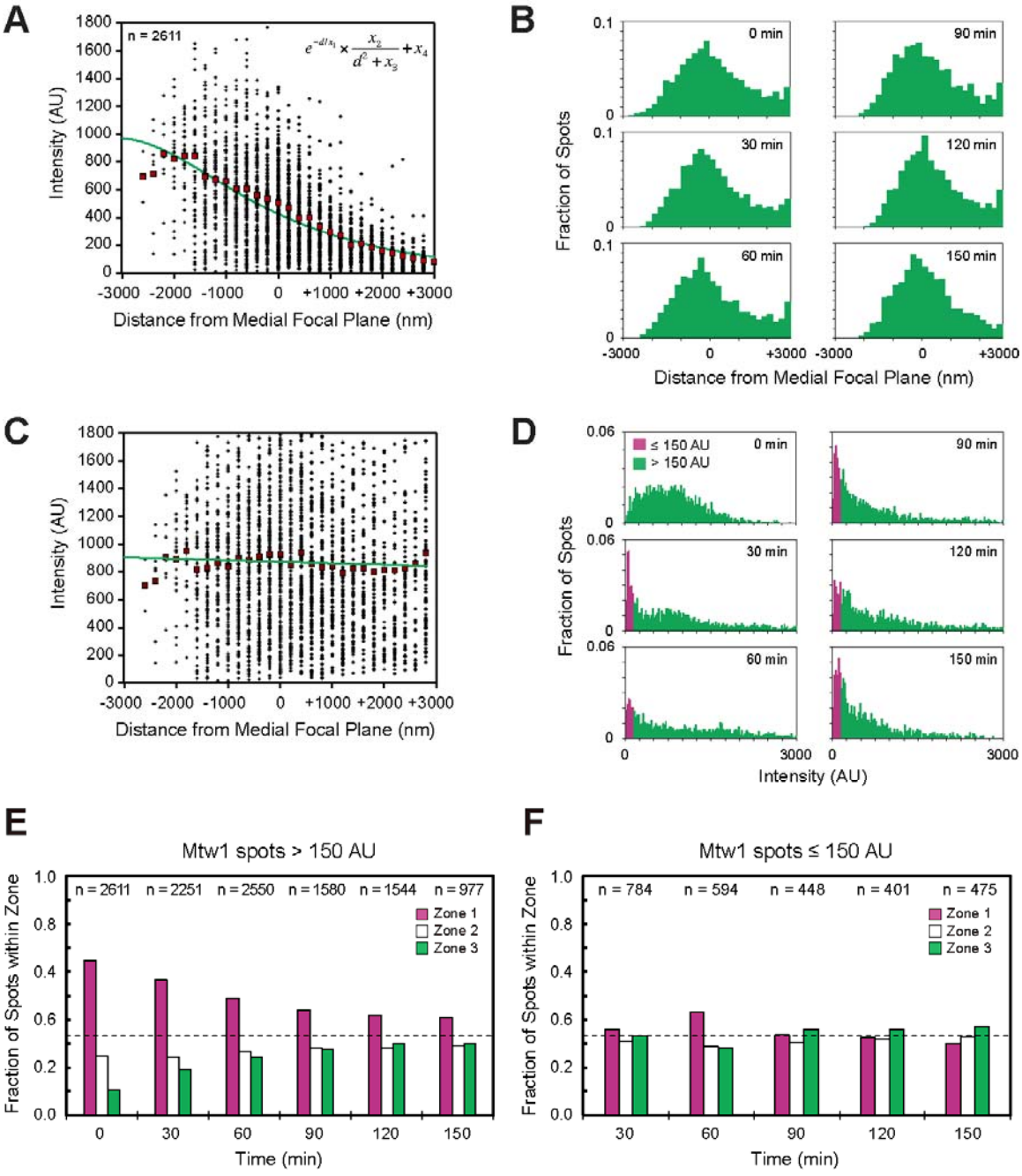

Figure S4. Analyses of the localization of detached kinetochores using Mtw1 intensity to identify detached kinetochores.

Attached kinetochores cluster due to their interactions with microtubules and appear as one spot when visualized by fluorescence microscopy due to the diffraction limit, so they appear brighter than individual detached kinetochores (see Figure 4A). We therefore used Mtw1 fluorescence intensity as a means of distinguishing detached kinetochores in cells lacking a fluorescent marker for SPBs. Cells expressing Mtw1-3×GFP and Nsg1-mCherry were exposed to nocodazole for 0 to 150 min before fixation and imaging by epifluorescence microscopy, taking 29 0.2-µm z-steps. **(A)** Fluorescence intensities of

individual Mtw1 spots at time zero, before addition of nocodazole, varied inversely with the distance of the spots from the objective lens. Green line depicts a least-squares fit to the data using the inset equation, which we used to correct fluorescence intensities across the z-axis. Red squares show the mean at each z-position. **(B)** Distribution of Mtw1 spots along the z-axis at each time point. We approximated the center of each distribution by Gaussian fitting to apply a time point-specific vertical offset to correct for small variations in specimen depth. **(C)** The relationship between Mtw1 spot depth and spot intensity after the z-position and intensity corrections described in (A) and (B). Green line depicts a linear regression and red squares show the mean at each z-position to highlight the adjustment to the distribution. **(D)** Mtw1 spot intensity distributions at each time point after applying the corrections illustrated in (C-E). Following treatment with nocodazole (30-150 min), spots were classified as "dim" (≤150 AU, magenta) or "bright" (>150 AU, green) (see Materials and Methods). **(E-F)** Subnuclear localization distribution of Mtw1 spots classified as "bright" (E) or "dim" (F). Dotted line at 33.3% represents the expected distribution if localization is random.

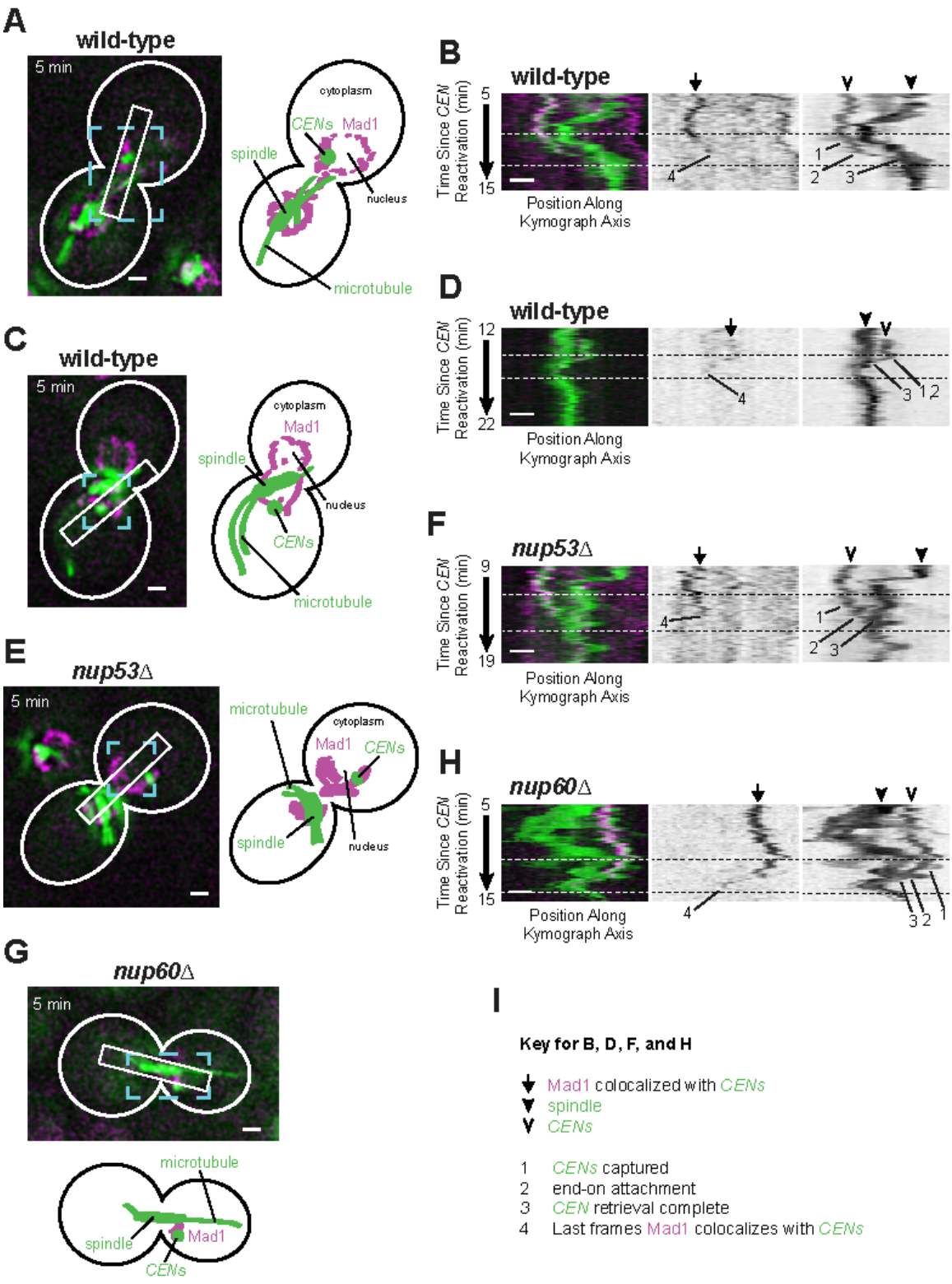

Figure S5. Analysis of Mad1 disappearance from centromeres following capture in wild-type, *nup53Δ*, and *nup60Δ* cells.

Additional analyses of the cells shown in Figure 5 and Video 3-6. **(A, C, E, and G)** First frames of movies (left) with the cell boundaries outlined in white, and cartoons of the images with features labeled (right), presented to aid interpretation. Blue boxes highlight the regions of interest shown in Figure 5. White boxes show the regions subjected to kymograph analysis in **(B, D, F, and H). (I)** Key for (B, D, F, and H). Scale bars, 1 μm.

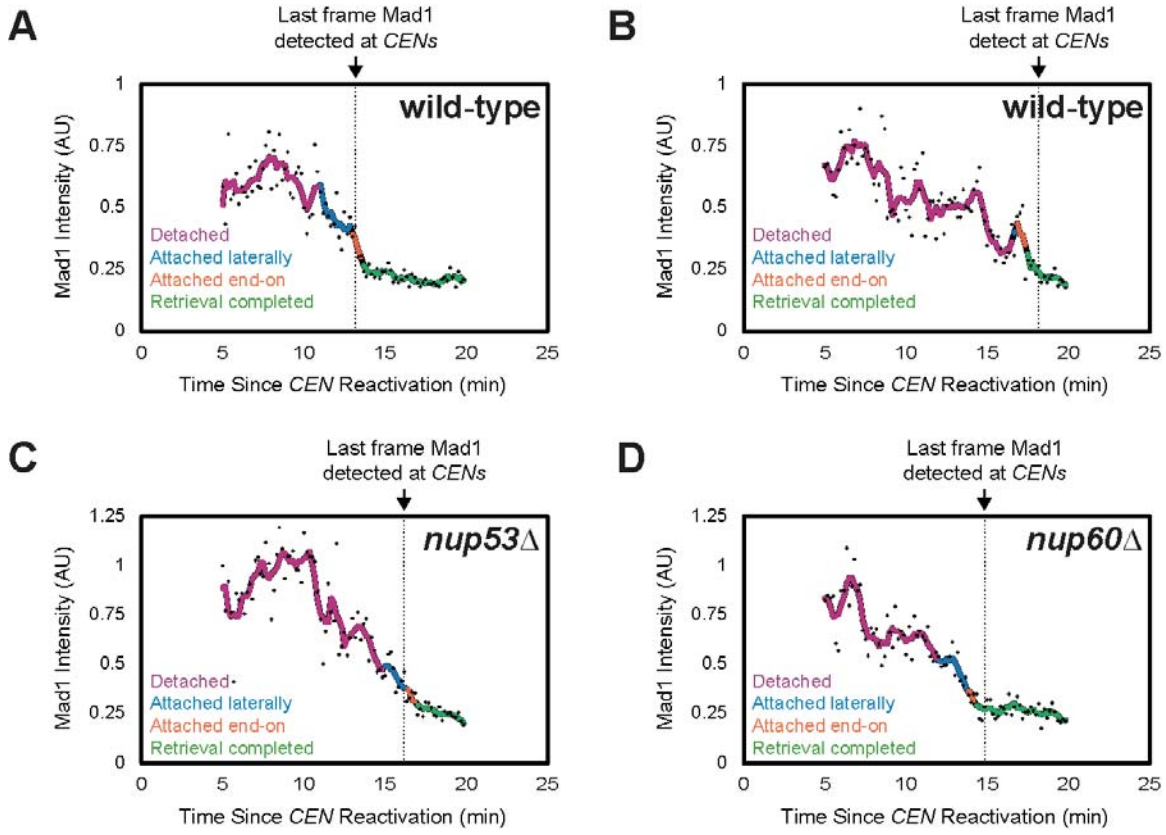

Figure S6. Quantification of Mad1 intensity at centromeres following capture in wild-type, *nup53Δ*, and *nup60Δ* cells.
Mad1 intensity at the centromeres of the wild-type **(A-B)**, *nup53Δ* **(C)**, and *nup60Δ* **(D)** cells shown in Figure 5A-E and S5 and Video 3-6, normalized by taking the ratio of the mCherry signal to the associated GFP intensity (dots). A color-coded sliding window average of five frames is also shown. Note that the timing of Mad1 disappearance for Figure 5F was judged by visual analysis of the microscopy data, not the fluorescence intensity trace.

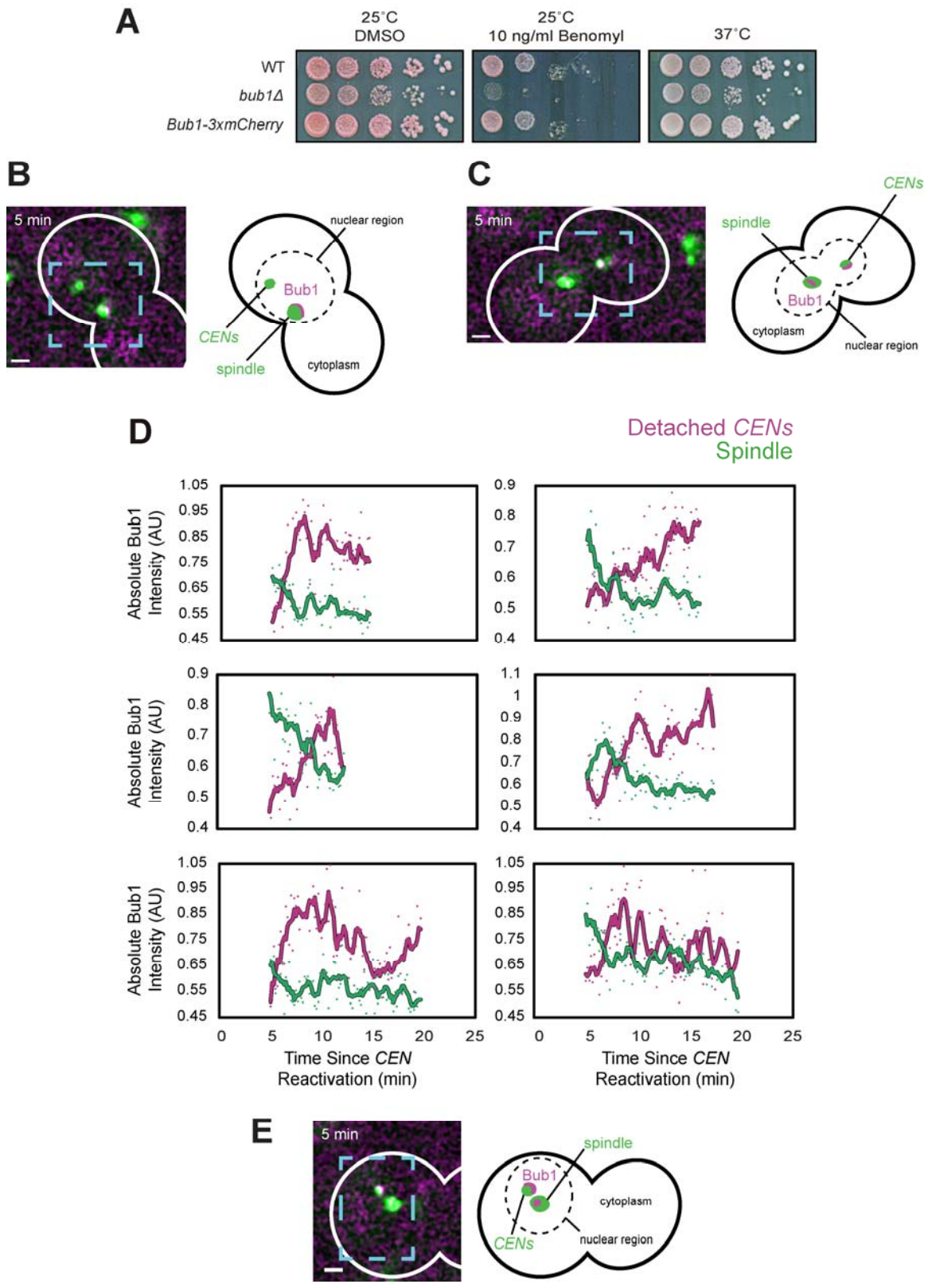

Figure S7. Analysis of Bub1 localization to kinetochores using the centromere reactivation assay.

Additional analyses of the cells shown in Figure 7-8 and Video 8-10. **(A)** Serial dilutions of wild-type, *bub1Δ*, and *BUB1-3×mCherry* yeast. **(B-C and E)** First frames of the movies (left) with the cell boundaries outlined in white, and cartoons of the images with features labeled (right), presented to aid interpretation. Blue boxes highlight the regions of interest shown in Figure 7-8. Scale bars, 1 μm. **(D)** Traces of the absolute intensity of Bub1 at the centromeres and spindle of several cells to illustrate that the accumulation of Bub1 at one site was frequently accompanied by the loss of Bub1 at the other site. Color-coded sliding window averages of five frames are also shown.

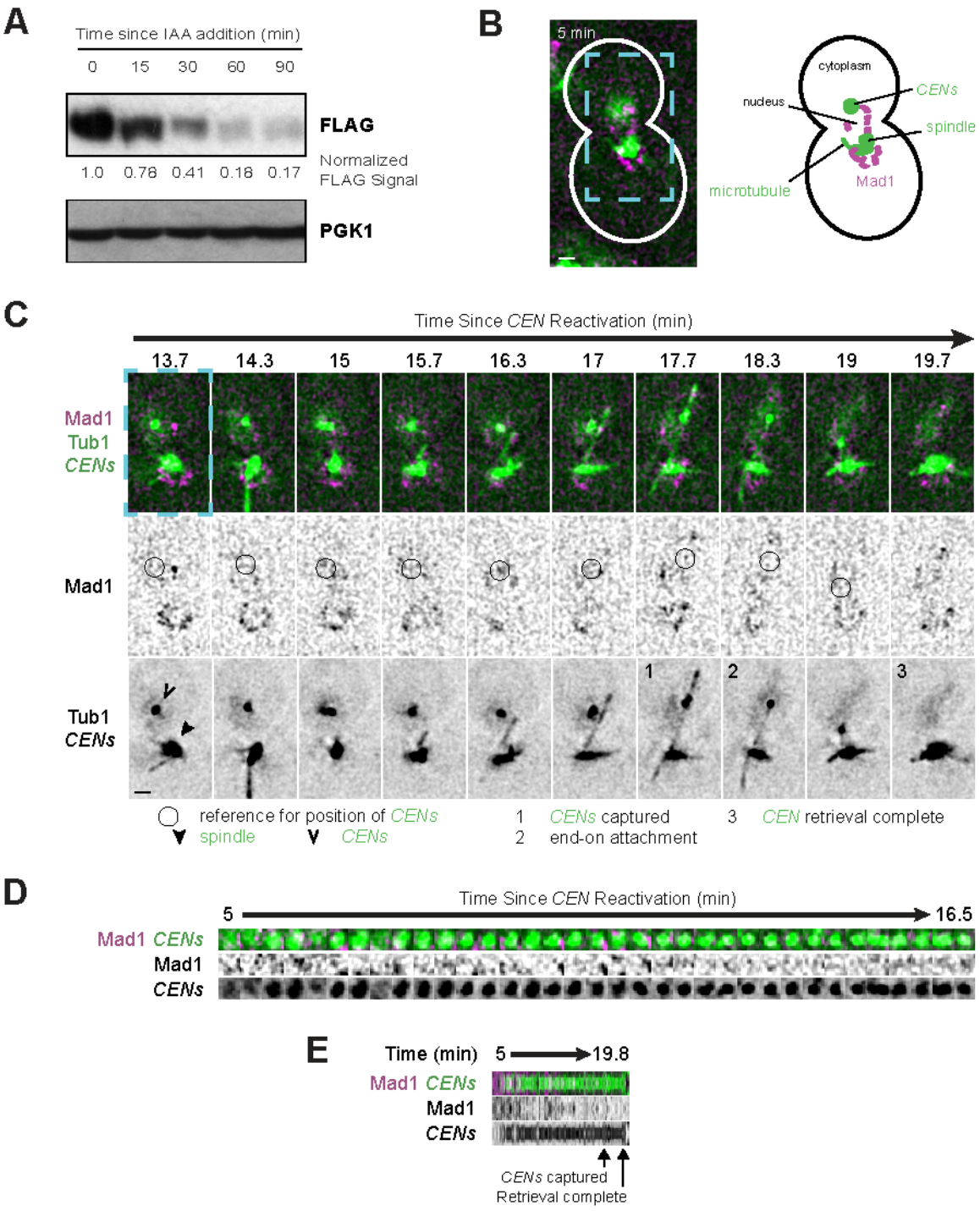

Figure S8. Consequences of Bub1 depletion for Mad1's centromere localization. Cells expressing Bub1-AID*-FLAG, OsTIR1-9xMYC, Mad1-3×mCherry, GFP-Tub1, and TetR-GFP and bearing *MET3pr-CDC20* and *GAL1pr-CEN3-TetOs* were first grown for 2.5 h at 25°C in YP medium plus 2 mM methionine, 2% raffinose, and 2% galactose to synchronize cells in metaphase and to inactivate *CEN3*. **(A)** Indole-3-aceitic acid (IAA) was added to 250 μM and lysates of the cells were subjected to immunoblotting at the given time points. **(B-E)** IAA was added to 250 μM for 60 min. The cells were then

released into synthetic medium plus 2 mM methionine and 250 μM IAA containing 2% glucose at 25°C to reactivate *CEN3* and then analyzed by epifluorescence microscopy beginning 5 min later, taking z-stacks every 10 sec. Representative deconvolved, Gaussian-filtered MIPs are shown. Scale bars, 1 μm. **(B)** First frame of the movie (left, Video 11) with the cell boundary outlined in white, and cartoon of the image with features labeled (right), presented to aid interpretation. Blue box highlights the region of interest shown in (C). **(C)** Time series from the same cell showing that Mad1 is not strongly recruited to the reactivated centromeres, although centromere capture and retrieval occurs normally. **(D)** Time series centered on the centromere to show the lack of continuous Mad1 colocalization with the centromere (20 sec/frame). **(E)** Kymograph made from 15 by 15 boxes approximately centered on the centromeres.

Table S1. Yeast strains used in this study.

Strain	Genotype	Source/Reference
DDY4554	*MATα his3 ura3 trp1 MET3pr-CDC20::TRP1 ade2::GFP-TUB1::ADE2 GAL1pr-CEN3-CYC1ter-tetO2x112::URA3 leu2::TetR-GFP::LEU2*	This study[a,b]
DDY983	*MATa ade2-1 his3-11 leu2-3,112 ura3-1 trp1-1(am)*	W303 wild-type
DDY4555	*MATa ade2-1 his3-11 leu2-3,112 ura3-1 trp1-1(am) mad1Δ::NatR*	This study
DDY4556	*MATa ade2-1 his3-11 leu2-3,112 ura3-1 trp1-1(am) MAD1-3xmCherry::LEU2*	This study
DDY4557	*MATα his3 ura3 trp1 MET3pr-CDC20::TRP1 ade2::GFP-TUB1::ADE2 GAL1pr-CEN3-CYC1ter-tetO2x112::URA3 leu2::TetR-GFP::LEU2 MAD1-3xmCherry::LEU2*	This study[a,b]
DDY4558	*MATa ade2 his3 leu2-3,112 ura3 trp1-1(am) bar1Δ::NatR MET3pr-CDC20::TRP1 GAL1pr-CEN3-CYC1ter-tetO2x112::URA3 MTW1-3xGFP::HIS3 MAD1-3xmCherry::LEU2 pRS412*	This study[a,c]
DDY4559	*MATα his3 ura3 trp1 MET3pr-CDC20::TRP1 ade2::GFP-TUB1::ADE2 GAL1pr-CEN3-CYC1ter-tetO2x112::URA3 leu2::TetR-GFP::LEU2 MAD1-3xmCherry::LEU2 nup53Δ::NatR*	This study[a,b]

DDY4560	*MATα his3 ura3 trp1 MET3pr-CDC20::TRP1 ade2::GFP-TUB1::ADE2 GAL1pr-CEN3-CYC1ter-tetO2x112::URA3 leu2::TetR-GFP::LEU2 MAD1-3xmCherry::LEU2 nup60Δ::NatR*	This study[a,b]
DDY4561	*MATa his3 ura3 trp1 MET3pr-CDC20::TRP1 ade2::GFP-TUB1::ADE2 GAL1pr-CEN3-CYC1ter-tetO2x112::URA3 leu2::TetR-GFP::LEU2 MAD1-3xmCherry::LEU2 mlp1Δ::KanMX mlp2Δ::SpHIS5*	This study[a,b,d,e]
DDY4562	*MATa his3 ura3 trp1 MET3pr-CDC20::TRP1 ade2::GFP-TUB1::ADE2 GAL1pr-CEN3-CYC1ter-tetO2x112::URA3 leu2::TetR-GFP::LEU2 MAD1-3xmCherry::LEU2 kar3Δ::KanMX4::kar3-64*	This study[a,b]
DDY4563	*MATα his3 ura3 trp1 MET3pr-CDC20::TRP1 ade2::GFP-TUB1::ADE2 GAL1pr-CEN3-CYC1ter-tetO2x112::URA3 leu2::TetR-GFP::LEU2 MAD1-3xmCherry::LEU2 dam1-1::KanMX*	This study[a,b]
CUY1846	*MATa ade2 his3-Δ200 leu2-3,112 ura3-52 MTW1-3xGFP::HIS3 SPC42-RFP::KanMX6*	Huang and Huffaker, 2006
DDY4564	*MATα ade2 his3-Δ200 leu2-3,112 ura3-52 bar1Δ::NatR MTW1-3xGFP::HIS3 NSG1-mCherry::KanMX6 SPC42-CFP::kanMX6 pRS412*	This study[c]
DDY4565	*MATa ade2 his3-Δ200 leu2-3,112 ura3-52 bar1Δ::NatR NSG1-mCherry::KanMX6 SPC42-GFP::kanMX6 pRS412*	This study
DDY4566	*MATα ade2 his3-Δ200 leu2-3,112 ura3-52 bar1Δ::NatR MTW1-3xGFP::HIS3 NSG1-mCherry::KanMX6 pRS412*	This study[c]
DDY4567	*MATa ade2 his3-Δ200 leu2-3,112 ura3-52 bar1Δ::NatR NSG1-mCherry::KanMX6 GAL::LacO::LEU2 his3::LacI-GFP::HIS3 pRS412*	This study[f]
DDY4568	*MATa ade2 his3-Δ200 leu2-3,112 ura3-52 bar1Δ::NatR NSG1-mCherry::KanMX6 GAL::LacO::LEU2 his3::LacI-GFP::HIS3 ada2Δ::KanMX pRS412*	This study[f]
DDY4816	*MATa ade2-1 his3-11 leu2-3,112 ura3-1 trp1-1(am) bub1Δ::NatR*	This study
DDY4817	*MATa ade2-1 his3-11 leu2-3,112 ura3-1 trp1-1(am) BUB1-3xmCherry::LEU2*	This study

DDY4818	*MATα his3 ura3 trp1 MET3pr-CDC20::TRP1 ade2::GFP-TUB1::ADE2 GAL1pr-CEN3-CYC1ter-tetO2x112::URA3 leu2::TetR-GFP::LEU2 Bub1-3xmCherry::LEU2*	This study[a,b]
DDY4819	*MATα his3 ura3 trp1 MET3pr-CDC20::TRP1 ade2::GFP-TUB1::ADE2 GAL1pr-CEN3-CYC1ter-tetO2x112::URA3 leu2::TetR-GFP::LEU2 MAD1-3xmCherry::LEU2 ura3-1::OsTIR1-9xMYC::URA3 BUB1-AID*-6xFLAG::HygMX*	This study[a,b,g]

[a] *ade2::GFP-TUB1::ADE2* derived from T5363 (Kitamura *et al.*, 2007)
[b] *leu2::TetR-GFP::LEU2*, *cen3::GAL1pr-CEN3-CYC1ter-tetO2x112::URA3*, and *MET3pr-CDC20::TRP1* were derived from T3531, *kar3Δ::KanMX4::kar3-64* was derived from T5058*, dam1-1::KanMX* was derived from T5057 (Tanaka *et al.*, 2007)
[c] *MTW1-3xGFP::HIS3* derived from CUY1846 (Huang and Huffaker, 2006)
[d] *mlp1Δ::KanMX* derived from KWY2691 (gift from Karsten Weiss)
[e] *mlp2Δ::SpHIS5* derived from DLY6927 (Addinall *et al.*, 2011)
[f] *GAL::LacO::LEU2*, *his3::LacI-GFP::HIS3*, and *ada2Δ::KanMX* derived from KWY1758 (Green *et al.*, 2012)
[g] *ura3-1::OsTIR1-9xMYC::URA3* derived from SBY12504 (Umbreit *et al.*, 2014)

References

Addinall, S. G. *et al.* (2011). Quantitative fitness analysis shows that NMD proteins and many other protein complexes suppress or enhance distinct telomere cap defects. PLoS Genet. *7*, e1001362.

Green, E. M., Jiang, Y., Joyner, R., and Weis, K. (2012). A negative feedback loop at the nuclear periphery regulates GAL gene expression. Mol. Biol. Cell *23*, 1367–1375.

Huang, B., and Huffaker, T. C. (2006). Dynamic microtubules are essential for efficient chromosome capture and biorientation in S. cerevisiae. J. Cell Biol. *175*, 17–23.

Kitamura, E., Tanaka, K., Kitamura, Y., and Tanaka, T. U. (2007). Kinetochore microtubule interaction during S phase in Saccharomyces cerevisiae. Genes Dev. *21*, 3319–3330.

Tanaka, K., Kitamura, E., Kitamura, Y., and Tanaka, T. U. (2007). Molecular mechanisms of microtubule-dependent kinetochore transport toward spindle poles. J. Cell Biol. *178*, 269–281.

Umbreit, N. T., Miller, M. P., Tien, J. F., Ortolá, J. C., Gui, L., Lee, K. K., Biggins, S., Asbury, C. L., and Davis, T. N. (2014). Kinetochores require oligomerization of Dam1 complex to maintain microtubule attachments against tension and promote biorientation. Nat. Commun. *5*, 4951.